Journal of Nuclear Materials 540 (2020) 152383

Contents lists available at ScienceDirect

Journal of Nuclear Materials

journal homepage: www.elsevier.com/locate/jnucmat

The role of ternary alloying elements in eutectoid transformation of U−10Mo alloy part II. *In* and *ex-situ* neutron diffraction-based assessment of eutectoid phase transformation kinetics in U-9.8Mo-0.2X alloy (X = Cr, Ni or Co)

N.E. Peterson [a, *], D. Malta [a], S.C. Vogel [b], B. Clausen [b], S. Jana [c], V.V. Joshi [c], S.R. Agnew [a]

[a] Materials Science and Engineering Department, University of Virginia, USA
[b] Materials Science and Technology Division, Los Alamos National Laboratory, Los Alamos, NM, 87545, USA
[c] Pacific Northwest National Laboratory, Richland, WA, 99352, USA

ARTICLE INFO

Article history:
Received 3 April 2020
Received in revised form
23 June 2020
Accepted 5 July 2020
Available online 15 July 2020

Keywords:
Phase transformation
Kinetics
Discontinuous precipitation
Rietveld
Neutron diffraction
Metallic fuels

ABSTRACT

Exploring the effects of minor ternary alloying additions, typically impurity elements, on the phase stability of U−10Mo is important for preventing undesirable phase decomposition during processing or during service. This work examines the influence small ternary additions of Cr, Ni, and Co. Both in-situ and ex-situ neutron diffraction measurements made during and after high temperature (450−525 °C) exposures were used to better define the influence of these elements on the time-temperature-transformation (TTT) behavior of U−10Mo, providing information which is complementary to electron microscopy investigations of the same alloy systems performed in the first part of this work. Minor additions of Ni and Co decrease the γ-phase stability at all temperatures investigated. Signatures of U_6X (X = Ni or Co) compounds were shown to be present in amounts of up to 6 wt% in the heat treated alloys, suggesting that the initial precipitation of this phase may catalyze further γ-phase decomposition. On the other hand, the Cr containing alloys were observed to have nearly the same, and in some cases slower, phase transformation kinetics when compared to the binary U−10Mo control samples. The results of the study have enabled preliminary estimates of the TTT curves for the ternary alloys.

1. Introduction

The development of suitable replacement fuels for research reactors and radioisotope production facilities has been a primary focus of the U.S. Department of Energy National Nuclear Security Administration's Office of Conversion within the Office of Material Minimization and Management, to convert research reactors from the use of highly enriched uranium (HEU) fuels to using low enriched uranium (LEU) fuels as part of nuclear non-proliferation efforts. However, the use of LEU fuels requires an increase in the uranium loading density in the fuel in order to obtain similar fuel performance to that of HEU fuels [1,2]. In addition to the uranium loading, two additional criteria of candidate LEU fuels must be evaluated in order to determine if a candidate fuel is a suitable replacement for HEU fuels; the burnup characteristics and phase stability during processing and in-reactor use.

Pure metallic uranium would provide the highest uranium density for fuel. However, below 667 °C, the equilibrium allotrope is the α-U phase, which has unfavorable burnup characteristics (cavitation swelling, thermal growth under power ramping) and microstructural stability during thermal cycling (thermal ratcheting) due to the anisotropy of the orthorhombic crystal structure [3,4]. The high-temperature (>774.8 °C) γ-U allotrope is a body-centered cubic structure and has more favorable irradiation characteristics [5]. Several 4d and 5d transition elements (e.g. Mo, Nb, V) have been shown to form solid solutions the γ-phase which can be retained in a metastable state upon quenching [2,6]. In particular, uranium-molybdenum alloy systems have been extensively studied as candidate LEU fuels due to the low temperature stabilization of the γ-phase of U, while also having a wide range of Mo solubility in the γ-phase of U, which allows fuel designers to balance between uranium density and γ-phase stability. Below the

* Corresponding author.
E-mail address: np7ut@virginia.edu (N.E. Peterson).

https://doi.org/10.1016/j.jnucmat.2020.152383
0022-3115/

eutectoid temperature, at approximately 560 °C, the γ U–Mo phase is metastable and will undergo a eutectoid decomposition to the α-U phase and the body-centered tetragonal U_2Mo phase, which is frequently denoted γ' because its unit cell resembles a stack of 3 ordered body-centered unit cells, resulting in a lattice where every third plane consists of Mo atoms. The presence of the α-U phase due to this transformation is detrimental to the fuel performance and must be tightly controlled during fuel processing.

Prior studies have investigated the effect of in-reactor irradiation on this phase transformation, indicating that the γ U–Mo phase is also stabilized at irradiation levels that are expected in high-performance research reactors [7,8]. Therefore, the case of unirradiated material may be considered as a "worst case scenario" with respect to phase stability. The current neutron diffraction-based study is designed to augment previous studies of U-10 wt% Mo phase stability [7,9–12], and in addition, it is expected to assist manufacturers and reactor operators by providing guidance with respect to critical times and temperatures to avoid by providing hitherto unavailable data for time-temperature-transformation (TTT) diagrams of the ternary alloys. In particular, the effect of dilute ternary alloying additions has been investigated in an effort to address the two following questions: Does the addition of various ternary elements (Co, Cr, or Ni) either; a) suppress unwanted phase decomposition during processing or service conditions or b) give rise to deleterious effects on phase stability? These common 3d transition elements were chosen based on prior work by Hofman et al., which showed that certain 4d and 5d transition elements could increase the γ-phase stability as ternary additions in U–Mo alloys [2]. In particular, both Pd and Pt (fcc) were shown to have the strongest stabilizing effect, while Ru and Os (hcp) also stabilize the γ-phase to a lesser effect. Cr was chosen because it has the same crystal structure as the γ-phase, bcc.

2. Background

The isothermal eutectoid transformation occurs in a variety of alloy systems, and for the U–Mo system it can be represented in the following form:

$$\gamma \rightarrow \alpha + \gamma' \quad (1)$$

where a supersaturated metastable phase (γ) decomposes to two thermodynamically stable phases (α+γ') to form the lamellar microstructure behind a moving grain boundary [13,14]. In case of the U–10Mo alloy system, it has been noted that in order to attain this equilibrium state it undergoes a discontinuous precipitation (DP) sequence, wherein the supersaturated γ-phase decomposes into a new lamellar microconstituent with alternating sections of a Mo-rich γ-phase (γ_b) and the α-U phase, which is practically Mo-free. At longer times, the γ_b phase further decomposes to γ'-U_2Mo [9]. Such DP-type phase transformations occur due to: local reductions in the free energy barrier for nucleation at the grain boundaries where precipitation begins, the minimization of the required diffusion path lengths due to the lamellar structure of the reaction product, and the high diffusivity path provided by the moving grain boundary. Solute segregation at the grain boundaries has been theorized to slow DP kinetics in various alloy systems, due to a solute drag effect of reducing the grain boundary energy (and thereby reducing the energetic benefit of grain boundary nucleation) and reaction interface mobility, thereby slowing growth kinetics [13,14]. Devaraj et al. hypothesized that Ni and Al rich complexions with Si-rich grain boundary precipitates can suppress the DP transformation in the U–10Mo system [15]. In part 1 of this work, Jana et al. studied the effect of small ternary additions of Co, Cr or Ni on the γ-phase stability using *ex*-situ x-ray diffraction and scanning electron microscopy [16]. It was shown that Ni and Co destabilize the γ-phase leading to more rapid phase transformation kinetics at 500 °C, while the Cr addition resulted in the slowest transformation kinetics in the ternary alloys at 500 °C.

In order to understand the kinetic landscape, time-temperature-transformation (TTT) diagrams have been developed for various Mo-concentrations within the U–Mo system. These were drawn based upon a combination of optical metallography, resistivity, hardness, x-ray diffraction, and dilatometry measurements, dating back to the 1950s [7,10,11,12,17–19]. In general, the phase transformation in the U–Mo alloys investigated (5–14.8 wt%Mo) exhibited the fastest transformations (commonly referred to as the "nose" of the TTT diagram) around 500 °C. However, large disagreements in the time for the transformation start exist, varying from 1hr to 30 h s. More recently, in-situ and ex-situ neutron diffraction have been demonstrated as an alternative to the classical methods mentioned above for kinetic studies [20,21]. Neutron diffraction combines high penetration with beam spots on the order of 1 cm and therefore offers probed volumes of ~1 cm in most materials. Even for high Z materials such as uranium and its alloys, neutrons offer superior grain counting statistics relative to surface-limited techniques such as x-ray diffraction or microscopy. This is particularly important for studying cast and homogenized alloys presently of interest because they exhibit grain sizes in the range of ~100 μm [22].

3. Experimental methods

Materials for this experiment were prepared at Pacific Northwest National Laboratory (PNNL) and transported to Los Alamos National Laboratory (LANL) for neutron diffraction measurements. The details of the fabrication of the same can be found in part 1 of this paper [16]. Four different compositions were evaluated in this work: U-10 wt%Mo, U-9.8 wt%Mo-0.2 wt%Cr, U-9.8 wt%Mo-0.2 wt%Ni, and U-9.8 wt%Mo-0.2 wt%Co. For each composition, three arc-melted buttons were created (12 total), which were subsequently cut into smaller pieces for the neutron diffraction experiments. A master U-9.2 wt%Mo was used during the arc-melting and 0.6 wt% Mo and 0.2 wt% of a ternary alloying element were added in order to reach the desired composition. For the U–10Mo control samples, 0.8 wt% of Mo was added instead. First, the samples were melted and arc-cast in a water-cooled copper hearth under vacuum with Ar gas backfill. Each alloy sample was then heated to 900 °C under argon gas for 48 h to homogenize the material, followed by a furnace cool. This step is critical because it both increases the homogeneity of the alloy chemistry and also brings the material well into the γ-phase field (>560 °C) of the phase diagram so that the material is fully converted to the BCC γ-phase in case any other phases had formed during casting. After this heating step, the material was furnace cooled, with an average cooling rate of ~2–3 °C during the critical temperature range of interest (600–400 °C).

For the *ex*-situ experiments, each of the were cut equally into two pieces, yielding a total of 24 total samples that were then subsequently heat-treated at one of three temperatures (450, 500 or 525 °C) for two different times (20 and 100 h). These temperatures were chosen in order to cover both the upper (525 °C), lower (450 °C) and nose (500 °C) regions of the currently accepted TTT curve of binary U–10Mo [12]. The samples were measured at room temperature on the **HI**gh **P**ressure **P**referred **O**rientation (HIPPO) beamline at the Lujan Center at Los Alamos Neutron Science Center. Data were collected at three unique sample rotations (ω = 0, 67.5, 90°) to enable a quantitative texture analysis in addition to quantitative phase analysis of each sample via Rietveld pattern refinement, using the program MAUD [23]. Count times were adjusted to be either 10 or 20 min per rotation for a proton current of 100 μA,

thus compensating for proton beam fluctuations. The 10 or 20 min were chosen depending on sample volume, resulting in total beam times of 30 or 60 min per sample. HIPPO is a time-of-flight neutron diffraction beamline, which enables a wide range of wavelengths to be collected by a total of 1200 ^{3}He detector tubes mounted on 45 panels on five detector banks arranged on rings located at nominal 2θ angles of 39, 60, 90, 120 and 144°. The large number of detectors, which each provide complete diffraction patterns spanning a significant range of plane spacings, are integrated for each panel, which enables relatively fast measurements with adequate resolution ($\Delta d/d$) to efficiently determine the phase composition and crystallographic texture of the samples. The 45 detector panels cover an area of ~22.4% of 4π with the three rotation providing diffraction data from ~51.7% of 4π [24], which is sufficient for reliable determination of the ODF. Although texture data was not a specific aim of the study, this capability ultimately provided a key insight described below. Sample were mounted on sample holders and loaded into a robotic sample changer [25] The neutron beam was collimated to 10 mm diameter using a boroncarbide collimator.

In addition to the ex-situ experiments, in-situ heating measurements were performed under vacuum on the **S**pectrometer for **MA**terials **R**esearch at **T**emperature and **S**tress (SMARTS) [26] to determine the kinetics of phase decomposition on samples of each ternary alloy tested. In an attempt to reduce the total time required for 6 *in*-situ measurements, two samples were placed side by side onto a steel sample holder, as shown in Fig. 1. Each sample had a thermocouple attached, which was passed through an alumina washer. The alumina washer was used to isolate the sample from the steel sample holder to prevent unwanted thermal conduction. In addition to the thermocouple, the samples were wrapped in niobium foil, which was used as an internal temperature standard, since the thermal expansion measured from lattice strain can be directly correlated to temperature through the known thermal expansion behavior. Prior to each experiment, the samples were aligned to ensure that the alumina washer and steel sample holder were not placed in the beam, to avoid additional diffraction peaks from these materials. For each experiment, the vacuum furnace chamber was heated to ~650 °C at the maximum ramp rate (50 °C per minute) and held for 1 h to calibrate the thermocouples and to re-solutionize the samples. After this step, the samples were furnace cooled down to the desired temperature and held for the time listed as follows; 500 °C for all of the samples, where the U−10Mo binary and Co ternary were held for 20 h and the Cr and Ni ternary were held for 30 h. The Cr and Ni ternaries were held for a longer period due a neutron beam outage during the test. During the experiment, the holder was moved horizontally in and out of the beam using the load frame actuator.

4. Analysis

Rietveld analysis of the *ex*-situ neutron diffraction data collected at HIPPO was performed using two programs; the Materials Analysis Using Diffraction (MAUD) software package, version 2.8, and the General Structure Analysis System package, with automated scripts using *gsaslanguage* [27–29]. MAUD was primarily used to analyze the texture of the different phases present as it has many options for texture quantification (E-WIMV, spherical harmonics, standard functions) and can accommodate the large number of spectra collected at HIPPO for simultaneous refinement of the patterns. For MAUD, the datasets were binned by detector panel, for a total of 45 spectra per measurement rotation and a total of 135 diffraction patterns per sample. MAUD has a built-in import wizard for HIPPO data, which loads each spectrum in with a 3rd order polynomial background function and groups the spectra by scattering angle into the aforementioned 5 detector banks (located at $2\theta \approx 39°, 60°, 90°, 120°$ and 144°). The d-spacing was limited from 0.5 to 3.5 Å during the analysis of data obtained from HIPPO using MAUD.

During the import process for MAUD, each individual spectrum was assigned a general scale factor which was refined [23]. As a final refinement step, the texture of the pure Mo phase, if present, was refined. None of the other phases exhibited strong intensity variations as a function of scattering and azimuth angle, which was confirmed with initial refinements of the texture of the γ-U phase, as shown in Fig. 4b. For all texture refinements, the E-WIMV algorithm present in MAUD was utilized, with a 15° discrete ODF cell size and no sample symmetry imposed. The pole figures presented in this paper were re-plotted for consistency using the MTex MATLAB™ toolbox after export of the calculated pole figures from MAUD [30].

For the analysis using GSAS, the datasets were binned by detector ring, resulting in a total of 5 spectra per measurement rotation, and the three rotations were subsequently summed together to provide the best counting statistics with the given datasets. This processing also randomizes weak to moderate preferred orientations, avoiding preferred orientation effects in the

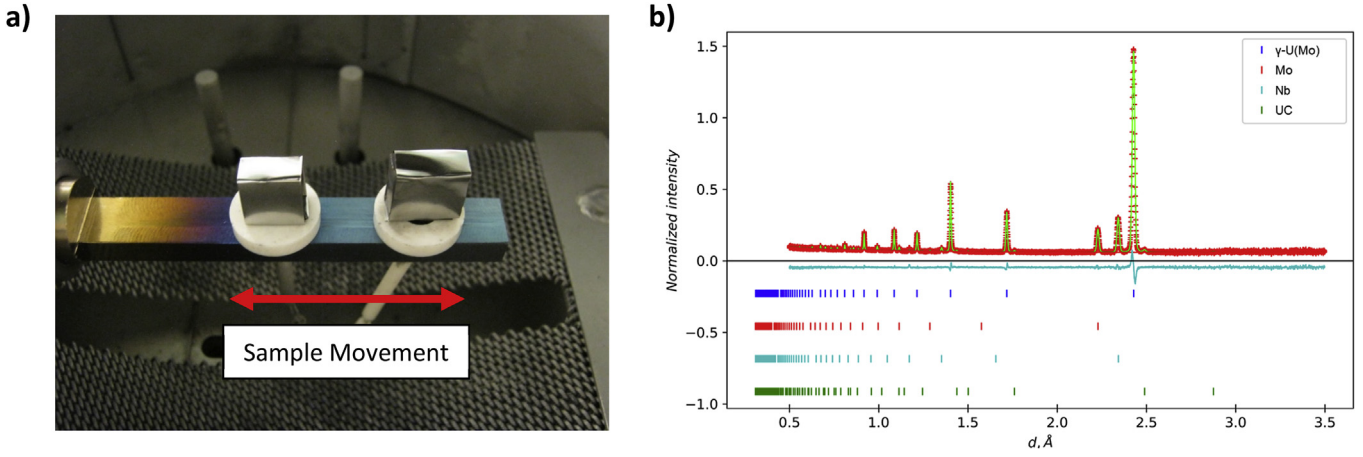

Fig. 1. a) U-9.8Mo-0.2Co (left) and U−10Mo (right) samples wrapped with niobium foil with a furnace control thermocouple attached. The sample holder is rastered laterally to change the sample into the neutron beam. **b)** Diffraction pattern and Rietveld fit obtained from the −90° bank at SMARTS, for the U-9.8Mo-0.2Ni sample (#12), collected prior to the in-situ experiment.

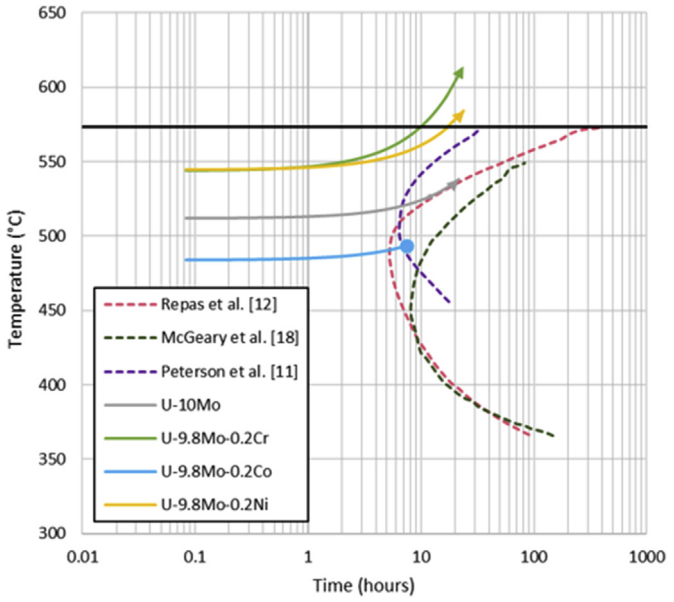

Fig. 2. TTT diagram with transformation start curves from Repas et al. [12], McGeary et al. [18] and Peterson et al. [11] for comparison with in-situ SMARTS data. Only the U-9.8Mo-0.2Co sample exhibited initial signs of eutectoid transformation with the presence of α and a Mo-rich γ-phase and this point is indicated by the filled circle. The approximate eutectoid temperature (~573 °C) for U−10Mo is shown with the black solid line.

subsequent analysis assuming a random crystallite orientation. For this analysis, the low resolution detector ring at $2\theta = 39°$ was excluded and the full d-spacing range accessible by each detector ring was used in the analysis. (min d-space: 0.4 Å, max d-space: 4.8, 6.0, 5.0, 7.5 for the 144°, 90°, 120° and 60° bank respectively). A gsaslanguage script was used to analyze all 24 datasets, thus ensuring identical data analysis. Besides background, histogram scale, absorption, phase weight fractions and lattice parameters for phase above 5 wt % and peak widths for phases above 10 wt% were refined. For all of the phases except γ-U and γ′-U_2Mo, the isotropic Debye-Waller (DW) factors (B_{iso}) were taken from prior experimental data: For the α-U, Mo, UC phases, literature values of 0.1891, 0.2169 and 0.19 $Å^2$ were used, respectively [31−33]. Considering the similarities of the crystal structures of both U_6Co and U_6Ni, the published DW factors for U_6Ni were used for both phases [34]. For the GSAS refinements, the atomic displacement parameters were refined for the γ-U and γ′-U_2Mo phases while being constrained to be equal. An estimate of the DW factor for the γ-U phase was obtained from refinements using MAUD of the nearly single phase (>98 vol% γ-U) U−Mo samples that were heat treated at 450, 500 and 525 °C for 20 h, and the average DW factor was found to be 1.31 ± 0.43 $Å^2$. For the MAUD refinements, the DW factors for the γ-U and γ′-U_2Mo phases were set to 1.31 $Å^2$ and 0.25 $Å^2$, respectively and not refined.

The *in*-situ neutron diffraction data collected at SMARTS were analyzed using the *GSAS-II* software package, utilizing the functionality for sequential refinement of diffraction spectra [35]. For the sequential refinement, an initial pattern is fit to obtain initial values for phase parameters (scale factors, unit cell dimensions) and the background function (6th order Chebyshev polynomial). These initial parameters are refined and then used as starting values for the next pattern in the sequence and so on. This process repeats until each pattern in the sequence is refined. For these refinements, the d-spacing range was limited from 0.5 to 3.5 Å.

For data from both instruments, the phases present in these samples include the orthorhombic α-U, bcc γ-U solid solutions, the body centered tetragonal (bct) γ′-U_2Mo intermetallic phase and small amounts of rocksalt-structured uranium carbide (present from the sample production). In the Co- and Ni-containing ternary alloys, the bct U_6Co and U_6Ni intermetallic phases, respectively, were also detected. As discussed in greater detail below, it was

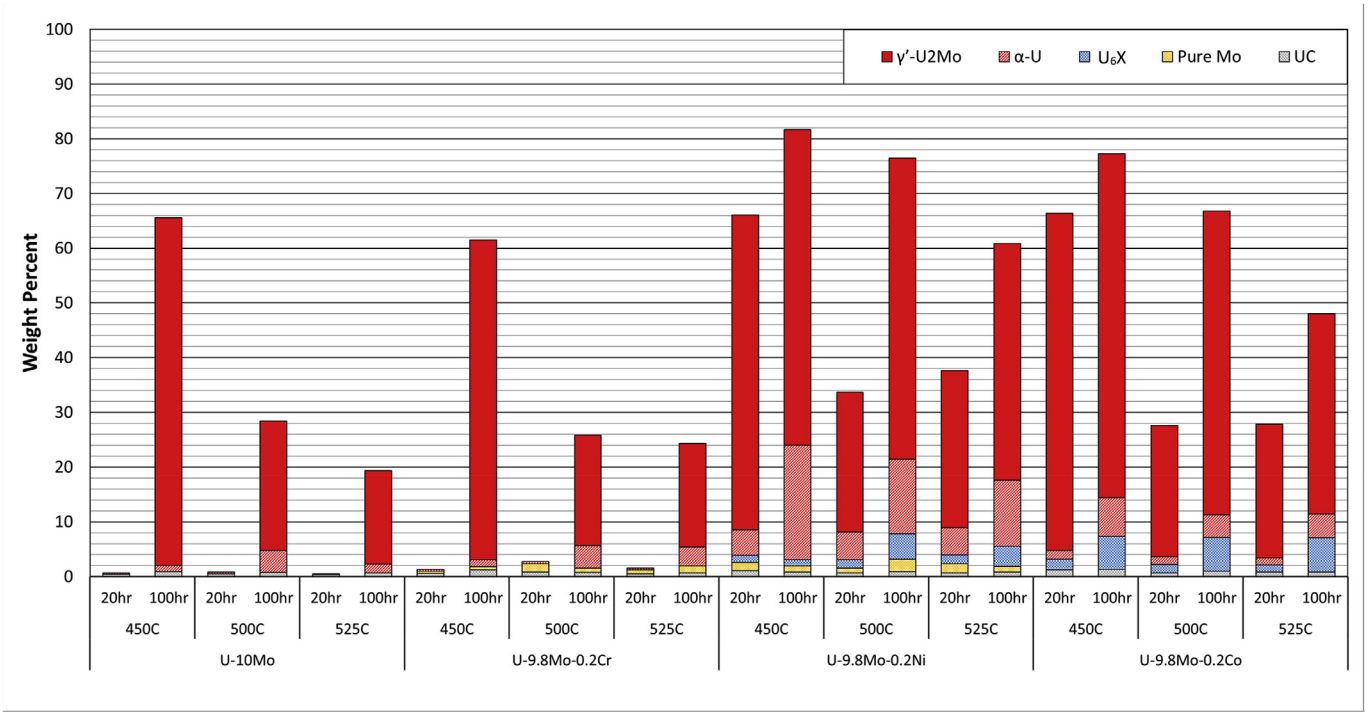

Fig. 3. Weight percentages phases present in each sample (the remainder is the γ-phase U solid solution in each case). Both uranium carbide (UC) and pure molybdenum (Mo) are plotted on the bottom of each bar if present in the sample for consistency. The order of phases (top to bottom) in each bar plot follows the order of listing in the legend (left to right).

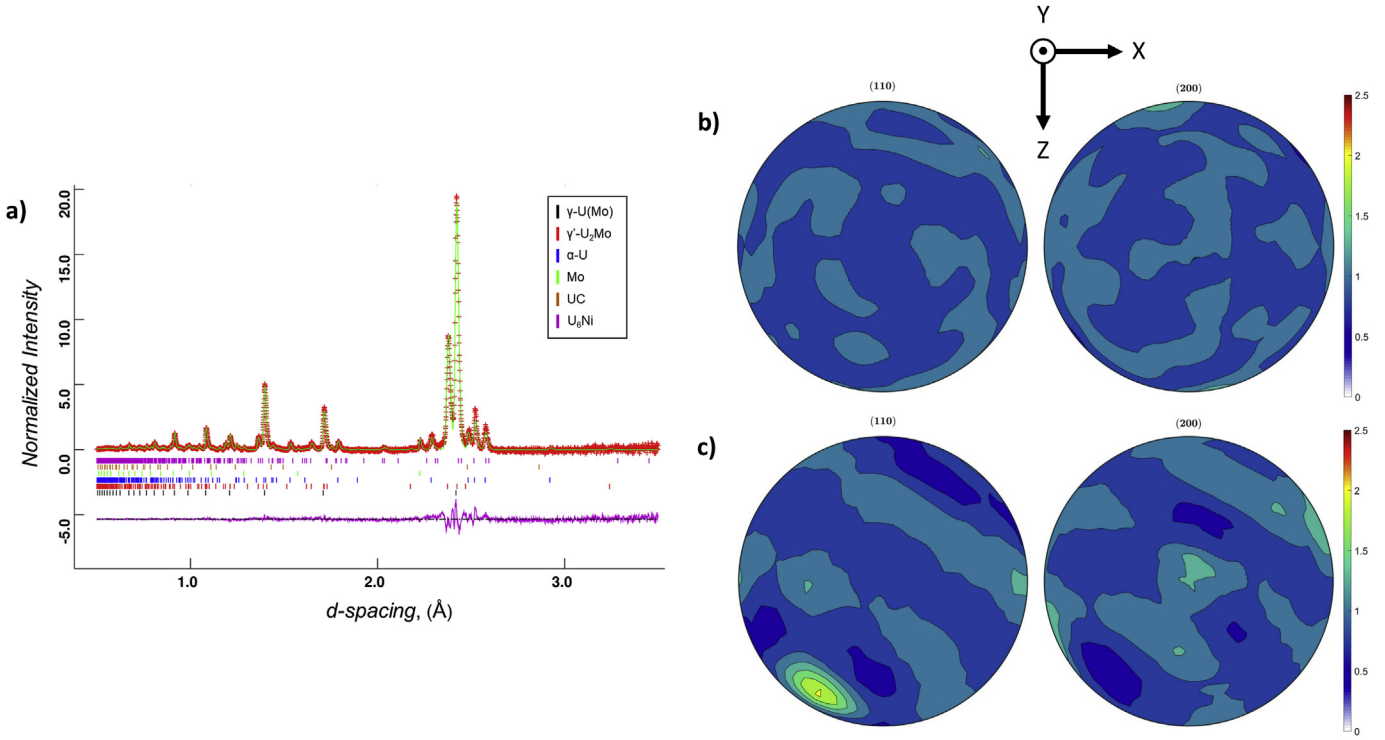

Fig. 4. a) Diffraction pattern averaged from all of the detectors in a ring located at 144° 2θ on HIPPO, for the U-9.8 wt%Mo-0.2 wt%Ni sample heat treated at 525 °C for 100 h s. (110) and (200) pole figures calculated from the same sample for the **b)** γ-U phase and **c)** Mo phase from the U-9.8Mo-0.2Cr sample #10. A typical <110> type fibre BCC drawing texture is present in the Mo pole figures, which indicates the stock Mo wire used is axially aligned at an angle of ~85° off the instrument y-axis in the sample.

discovered that small amounts of pure (undissolved) Mo existed (~0.8 wt%) in the Ni- and Cr-containing ternary samples. As with any Rietveld refinement analysis, careful consideration must be made with respect to the parameters that define the model from which the theoretical pattern is calculated. MAUD includes a refinement wizard feature that allows for automation; however, this method is not recommended by the current authors for use in complex analyses such as the present case. Hence, the method for refinement steps outlined by Wenk et al. [23] were followed as an outline, rather than using the refinement wizard. The crystallite size and microstrain parameters, which are related to peak breadth, were not refined for the texture analysis with MAUD due to the large degree of peak overlap, presence of several minority phases, and instability of the parameters during trial refinements. A profile fit with a R_{wp} value below 10% and was presumed to be a sufficient fit during the analyses.

5. Results

5.1. Ex-situ

The results of the Rietveld refinements of the 24 samples examined *ex-situ* on HIPPO are listed in Table 1 and shown in Fig. 3. During the analysis of the results, it was discovered that both the Cr and Ni containing ternary alloys had small amounts of pure Mo present, with an average of 0.7 wt% Mo being present across all of the U-9.8Mo-0.2Cr and U-9.8Mo-0.2Ni alloy samples. Furthermore, the crystallographic texture of the Mo phase was able to be reliably refined and is consistent with a <110> fiber texture, typical of a drawn BCC metal. This is consistent with the wire stock Mo that was used during the arc-casting of the buttons. In addition to the unmelted Mo, the matrix γ phase texture was also refined on the U–Mo sample heat-treated at 525 °C for 100 h and the results confirm the assumption that the matrix phase was not strongly textured, as expected for the sample processing history. An example diffraction pattern and recalculated pole figures for the γ and pure Mo phases are shown in Fig. 4. The phase transformation kinetics are in fact dependent upon Mo concentration (e.g., lower Mo content material exhibits faster transformations [11]). However, some firm conclusions can still be drawn from the present study.

Both the U−10Mo and U-9.8Mo-0.2Cr samples exhibit similar levels of transformation at all temperatures and times. After annealing at 450 °C for 100 h, the amount of γ' in the U-9.8Mo-0.2Cr sample was shown to be approximately ~5 wt% less than the U−10Mo sample at the same condition, indicating that Cr could have a small stabilization effect on the γ-phase as less transformation had occurred. Based on the knowledge of undissolved Mo being present in these samples, it is possible that Cr has a greater stabilizing effect on γ-phase in the sub-eutectoid temperature regime than reported in this study.

In contrast, the U-9.8Mo-0.2Ni and U-9.8Mo-0.2Co alloys exhibited much greater levels of transformation, even after a relatively short annealing time of 20 h when compared to the binary U−10Mo and U-9.8Mo-0.2Cr alloy. In particular, after 20 h at 500 °C, both the U-9.8Mo-0.2Ni and U-9.8Mo-0.2Co samples had similar phase fractions of α and γ' compared to phase fractions present in the U−10Mo and U-9.8Mo-0.2Cr samples after 100 h s at 500 °C. In the U-9.8Mo-0.2Ni samples, these high levels of transformation are also influenced by the presence of undissolved Mo, therefore the exact role of Ni in the γ-phase stability is somewhat unclear. Rest et al. compiled the γ-phase stability at 500 °C (transformation start time) and showed that U–Mo alloys have a linear relationship between uranium weight fraction in the alloy and γ-phase stability [36]. If we assume that all of the added Mo was not dissolved (U-9.2 wt%Mo), based on prior studies the transformation start time at 500 °C is predicted to be ~6.26 h, compared to ~7.58 h for a U-10 wt

Table 1
Weight fraction results from GSAS Rietveld refinements of the ex-situ data collected at HIPPO for each alloy and heat treatment combination. The column labeled "Before Experiment" for each sample represents the refinement results from data collected at SMARTS prior to the in-situ experiment. The niobium was only present in these samples, as it was used as a fiduciary thermocouple. The uncertainties are assumed to be ±0.6 wt% in all cases.

	U−10Mo							U-9.8Mo-0.2Cr						
	Before Exp.	20 h			100 h			Before Exp.	20 h			100 h		
		450C	500C	525C	450C	500C	525C		450C	500C	525C	450C	500C	525C
γ-U	87.5	99.3	99.2	99.5	34.5	71.6	80.7	85.3	98.6	97.3	98.5	38.5	74.2	75.7
γ′-U_2Mo	–	–	–	–	63.5	23.6	17.0	–	–	–	–	58.4	20.2	18.9
α-U	–	0.2	–	–	1.1	4.0	1.6	–	0.3	0.4	0.4	1.2	4.1	3.4
UC	0.9	0.4	0.5	0.4	0.9	0.8	0.6	1.0	0.6	0.8	0.5	1.3	0.7	0.7
γ-U (B2)	–	–	–	–	–	–	–	–	–	–	–	–	–	–
Pure Mo	–	–	–	–	–	–	–	2.2	0.4	1.6	0.7	0.5	0.8	1.3
Nb	11.6							11.5						
	U-9.8Mo-0.2Co							U-9.8Mo-0.2Ni						
	Before Exp.	20 h			100 h			Before Exp.	20 h			100 h		
		450C	500C	525C	450C	500C	525C		450C	500C	525C	450C	500C	525C
γ-U	82.2	33.6	72.4	72.2	22.7	33.2	52.0	82.7	33.9	66.3	62.4	18.3	23.5	39.2
γ′-U_2Mo	–	61.6	24.0	24.4	62.9	55.5	36.6	–	57.5	25.5	28.6	57.7	55.0	43.3
α-U	–	1.6	1.4	1.2	7.1	4.0	4.3	–	4.7	5.0	5.0	20.9	13.6	12.0
UC	0.8	1.2	0.7	0.8	1.3	1.0	0.8	1.2	1.0	0.7	0.7	0.9	0.9	0.9
U_6(Co,Ni)	1.4	2.0	1.5	1.3	6.0	6.2	6.3	–	1.3	1.5	1.6	1.1	4.7	3.7
Pure Mo	–	–	–	–	–	–	–	2.3	2.8	1.8	2.6	1.6	4.1	1.9
Nb	15.6							13.8						

%Mo alloy. This change is significant enough to prevent any conclusion as to whether it was in fact the Ni or the loss of Mo that was the cause for the decreased γ-phase stability. However, these results confirm that Co is in fact a γ-phase destabilizer, as previously indicated by studies employing x-ray diffraction and scanning electron microscopy [16].

Interestingly, at 450 °C after 100 h of exposure all of the alloys have significantly higher ratios of γ′-U_2Mo to α, which indicates that the nature of the phase transformation has changed at this lower temperature. These results are consistent with the classical TTT diagram composed by Repas [12], which shows a γ-γ′ region, in front of the α+γ′ region, starting at temperatures below approximately 425 °C. Jana et al. showed that during annealing of U−10Mo at 400 °C continuous precipitation of γ′ is in competition with the aforementioned discontinuous precipitation sequence, which is consistent with the results from this study [22]. Additionally, both the U−10Mo and the U-9.8Mo-0.2Cr samples contain a significant fraction of γ′ at 450 °C after 100 h s, with little or no α-U phase. On the other hand, the U-9.8Mo-0.2Ni samples and U-9.8Mo-0.2Co samples had large fractions of the γ′ phase with small amounts of the α after only 20 h, which indicates that Co is still an effective γ-destabilizer at lower temperatures. Further, from Table I, it is noted that the weight fraction of α-U is significantly higher in the case of U-9.8Mo-0.2Ni sample when compared to the U-9.8Mo-0.2Co sample at all of the temperatures and times tested. After 100 h of exposure at 450 °C, the U-9.8Mo-0.2Ni sample had 20.9 wt% α-U, which is more than what is present in the same alloy annealed at 500 °C and 525 °C for 100 h, e.g. ~13.6 wt% and 12.0 wt% respectively. A higher weight fraction of α-U in U-9.8Mo-0.2Ni sample annealed at 450 °C suggests an alternative precipitation mechanism, possibly continuous precipitation, to be active. However, the morphology of α-U formed through continuous precipitation should have an acicular morphology and should remain uniformly dispersed in the parent γ-phase parent matrix instead of the typical γ-UMo grain boundary initiated lamellar morphology associated with DP-based phase transformation route [37]. High resolution TEM imaging studies can confirm if such hypothesis are true.

The presence of very high U density phases was also observed in both the U-9.8Mo-0.2Ni and U-9.8Mo-0.2Co samples at all temperatures and times tested. The U_6X intermetallic BCT phases were present after 20 h, with an average of 1.5 ± 0.2 wt% U_6Ni and 1.6 ± 0.4 wt% U_6Co, respectively. The U_6Co phase fraction increased at all annealing temperatures from 20 h to 100 h of annealing time, while the U_6Ni phase fraction remained relatively constant with time only after annealing at 450 °C. An estimate of the Ni or Co remaining in solution can be made by calculating the element weight fraction of Ni or Co in the given phase, which has a known phase weight fraction. Both Ni and Co constitute 4.0 wt% and 4.0 wt % in the U_6Ni and U_6Co phases respectively, therefore if all of the 0.2 wt% of Ni or Co present in the sample were accounted for in the respective U_6X phase, approximately 5 wt% of the U_6X phase would be present. Based on the *ex*-situ results all of the samples annealed for 20 h at 450 °C, 500 °C and 525 °C had lower levels of the U_6X phase present, which suggests that the Co and Ni atoms are still dissolved into the other phases at this time. However, it is unclear if they are segregated to a single phase, accumulated as defects in grain boundaries, or are simply substitutional defects for Mo in all of the phases.

5.2. In-situ heating experiments on SMARTS

Unfortunately, during the analysis of the *in-situ* data it was determined that the temperature control of the samples was not constant, but rather slowly increased as the experiment went on. While the control and sample thermocouples both indicated constant temperatures, the niobium thermal expansion indicated that the sample temperature increased, on average, ~2−3 °C per hour. The time-temperature curves for each alloy tested are shown in the context of some classical TTT start curves [11,18] in Fig. 2. Only the Co-containing ternary alloy exhibited any evidence of the eutectoid transformation after ~7 ½ hour. The phase content of the other alloys remained unchanged, indicating that the boundaries of the actual TTT diagrams are not much different than those available in the literature despite the ternary alloying additions.

6. Discussion

The goal of this work is to determine phase fractions; however,

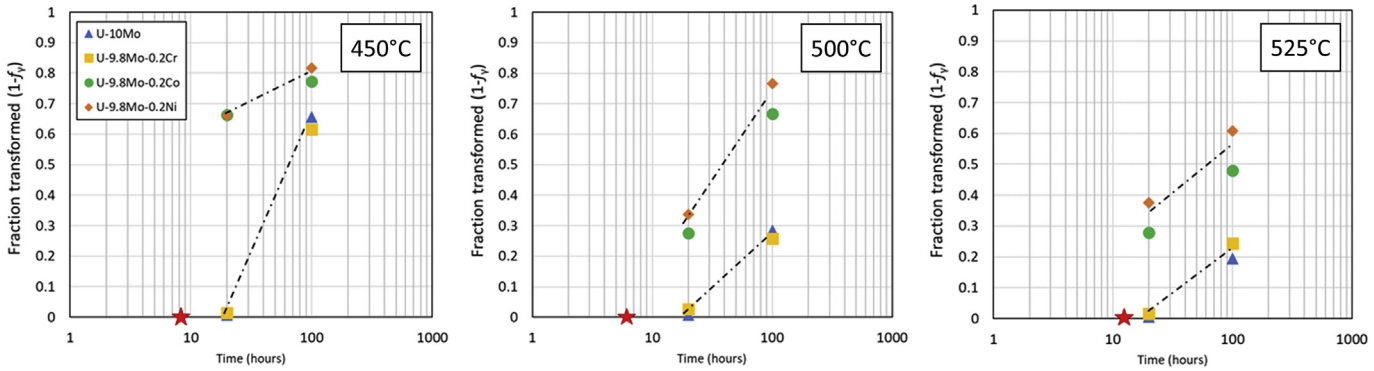

Fig. 5. Fraction transformed vs time for 450 °C (left), 500 °C (middle) and 525 °C (right). The drawn lines are meant as a guide to the eye for the two unique regimes for the samples, where the U−10Mo and U-9.8Mo-0.2Cr sample are in one regime and the U-9.8Mo-0.2Ni and U-9.8Mo-0.2Co are in another regime. The red star symbols indicate the transformation start time according to the U-10 wt%Mo TTT diagram presented by Repas et al. [12]. (For interpretation of the references to colour in this figure legend, the reader is referred to the Web version of this article.)

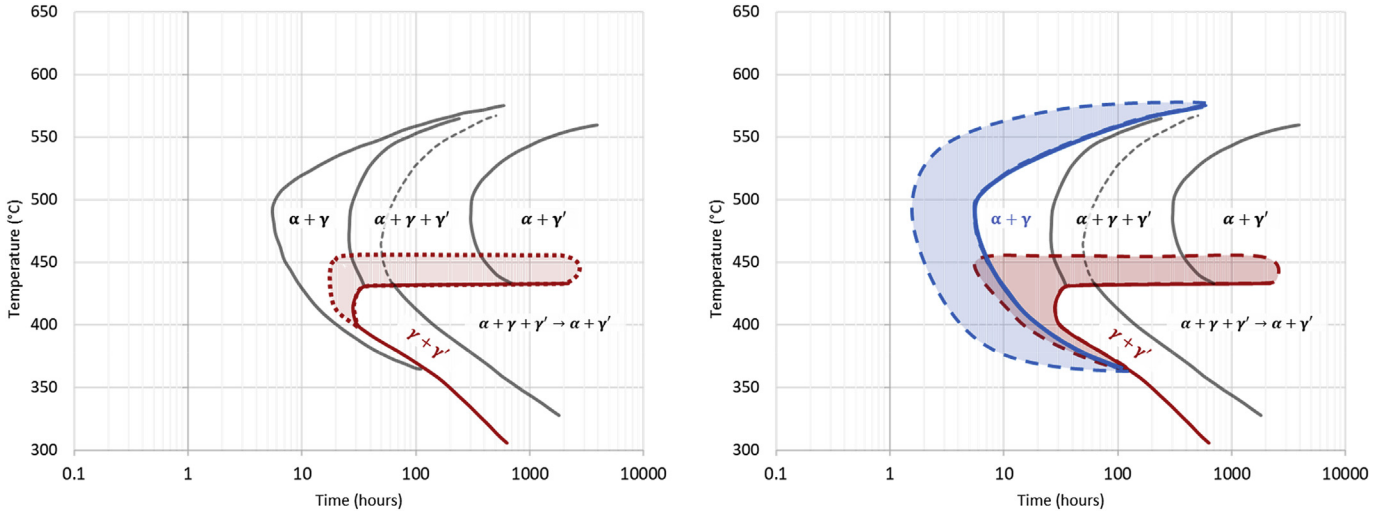

Fig. 6. TTT diagram recreated from Repas et al. [12], highlighting the suggested modifications based on results from this study for the U−10Mo (left) and U-9.8Mo-0.2Co (right). Predictions can only be made for these samples, due to undissolved Mo present in the other samples. The expanded $\gamma + \gamma'$-U_2Mo region and $\alpha + \gamma$ region are indicated with red and blue sections respectively. The dashed lines indicate the uncertainty in the true boundaries. (For interpretation of the references to colour in this figure legend, the reader is referred to the Web version of this article.)

the Bragg reflection intensities not only depend upon phase fractions but also crystallographic texture and thermal displacements and other factors. Although this complex deconvolution is the strength of a multiple whole-pattern Rietveld refinement, not all parameters can always be determined reliably from this procedure, especially for minority phases. If some of these parameters can be determined a-priori, then one can avoid false minima in the Rietveld solution which mistakenly attribute intensity changes to phase fractions, which are actually due to crystallographic texture and/or thermal displacements. Initial refinements of the datasets revealed that the γ-phase was not significantly textured (~1 M R.D.), and thus subsequent iterations did not refine the textures of the other majority phases (e.g. γ, γ' or α); only the texture of pure Mo phase was refined, if it was present (Fig. 4). The goodness of fit was initially poor and it was hypothesized that the thermal displacements of the various phases could be the cause for the discrepancies between the Rietveld model fit and experimental intensities.

The Debye-Waller factor or thermal (or atomic displacement) parameter, *D*, is a term that corrects the structure factor of a given reflection for the thermal motion of the atoms on the lattice sites [38]. Assuming the atomic thermal vibrations are isotropic,

$$D = \exp\left[-\frac{1}{2}u^2\left(\frac{4\pi \sin\theta}{\lambda}\right)^2\right] \quad (2)$$

where $\frac{4\pi \sin\theta}{\lambda}$ is the magnitude of the scattering vector and u^2 is the mean squared displacement of the atom with respect to its lattice site. In MAUD, GSAS, or GSAS-II, a user can enter the value for $B_{iso} = 8\pi u^2$ or u^2 of each atom of each phase directly. In this work, each site in a given phase was assigned the same value. Blanter et al. investigated the effect of Mo on the thermal displacements in uranium alloys by calculating u^2 vs temperature from theoretical calculations using an experimentally measured phonon dispersion curve [39]. They show that the presence of a significantly lighter solute atom into a heavy solvent introduces an additional line in the phonon spectrum; which lowers B_{iso} of the γ phase to below that of the two other allotropes of uranium, β-U (tetragonal) and α-U (orthorhombic), thereby stabilizing the γ-phase. Future studies should focus on either theoretical (via *ab*-initio methods, such as those used in Ref. [40]) or experimental determination of values for Biso for the phases present in this system; in particular the γ-U(Mo)

and γ′ phases, to improve the reliability of weight fraction determinations.

To contextualize the HIPPO *ex*-situ data, an initial inference into the kinetic behavior was attempted through a qualitative approach to a Johnson-Mehl-Avrami-Kolmogorov (JMAK) analysis. Although the classical TTT diagrams indicate a rich phase transformation sequence, in this work we are concerned mainly with the transformation start curve location, and therefore used (1 − vol. f_γ) as a total fraction transformed. The results from the *ex*-situ analysis are plotted for each temperature tested in Fig. 5a–c. In these figures, the approximate transformation start time based on the TTT diagram from Repas et al. [12] is shown with a star symbol, to provide context for comparison. Based on these plots, it is clear that the samples can be grouped into two regimes for each temperature, with the U–Mo binary & Cr ternary being in one regime and the Ni & Co ternaries being in the other. It is important to note that these plots are highly incomplete but serve to highlight potential areas for research in the future. It is *clear* that both the Ni & Co ternaries have faster kinetics in all three temperatures tested, however it is *unclear* as to where the exact transformation start begins. In both the U–Mo binary and Cr ternary, the data collected at 20 h for each temperature are very near zero. One exception was the data for the HT at 500 °C, (approximately the nose of the TTT curve), where (1 − vol. f_γ) was equal to 0.0469 and 0.054 respectively. If we can assume the JMAK curve follows a typical S shape, then it is most likely that in these samples the transformation start time is somewhere between 10 and 20 h, with the shortest time being at approximately 500 °C. Note that the currently accepted TTT diagram composed by Repas et al. shows the nose of the U–10Mo TTT diagram at approximately 490 °C, with a transformation start time of approximately 5.8 h. This is in agreement with the *ex*-situ data collected here for only the U–Mo binary and Cr ternary samples. However, the data collected for all of the samples at 450 °C suggest that the γ-γ′ region may in fact be present at higher temperatures, as each sample had significant γ′ phase fractions with very little or no α-U phase present. The proposed changes to the Repas TTT diagram are shown in Fig. 6. Although conclusions can not be made for the effect of Ni on the γ-phase stability due to the undissolved Mo present, the presence of the γ-γ' region at 450 °C is consistent between all of the samples and therefore it is not expected to be a strongly affected by small additions of Ni.

However, it must be noted that the transformation start time may still be a strong function of Ni ternary additions. In order to precisely determine the transformation start line more granular measurements would have to made, most likely down to 25 °C or smaller increments. The U–Mo and Cr ternary samples also show agreement with the Repas TTT diagram at 525 °C.

Another critical microstructural feature that must be considered when comparing the various TTT diagrams presented in the literature is the prior γ-phase grain size, which has been shown to influence the eutectoid transformation kinetics by many prior studies [37,41,42]. Repas et al. did not report a grain size, so a direct comparison is not possible. However, based on the material thermo-mechanical processing used in their study; extrusion, with a homogenization treatment of 980 °C for 4 h followed by a water quench with an additional hold at 900 °C for 1 h prior to the aging heat treatment, it is expected that the samples used in the present study have a larger average grain size, compared to the U-10 wt% Mo samples tested in the study by Repas et al. This could explain the discrepancy in the transformation start times, as a smaller grain size will increase the discontinuous precipitation kinetics due to the increased grain boundary area.

7. Conclusions

Ex-situ (and limited in-situ) time of flight neutron diffraction experiments performed on quenched samples of U-10 wt%Mo alloys with minor ternary alloying additions of Cr, Co, and Ni have revealed:

- Minor additions of Ni and Co have a detrimental effect on the γ-phase stability at all temperatures investigated. The exact role of Ni is slightly vague due to the undissolved Mo in U-9.8Mo-0.2Ni samples. Both Ni and Co led to occurrence of U_6M phases.
- The samples employed in this study were shown to have (~0.8 wt%) undissolved Mo in them, and therefore, the actual matrix composition is ~9.2 wt% Mo, which would render the γ-phase slightly less stable. Nevertheless, the phase transformation kinetics were quantitatively identical to the U-10 wt% Mo binary. This suggests that there is a possibility that Cr slightly slows the transformation. Note that binary U–Cr phase diagrams suggest that Cr stabilizes the γ-phase, similar to Mo and other refractory metals. No additional intermetallic phases were observed in this system.
- Significantly higher weight fractions of α-U were measured in U-9.8Mo-0.2Ni alloy, especially at 450 °C after 100 h of exposure. A continuous precipitation-type phase transformation is believed to be operative in the U–Mo system at lower temperatures (~450 °C). Thus, based on the present study, addition of a ternary element may change the kinetics of continuous precipitation-type phase transformation, in addition to the discontinuous precipitation kinetics as well. Further high resolution image based studies are needed to confirm this hypothesis.

A qualitative Johnson-Mehl-Avrami-Kolmogromov (JMAK) analysis suggested that future work should focus on investigating the short time (<20 h) phase transformation kinetics, especially with Ni or Co ternary additions, to determine a more precise transformation start time. Future work should also focus on investigating the region below the TTT nose (<500 °C), as the work presented here suggest an initial region of γ-UMo and γ′-U_2Mo, which is distinct from the phase transformation observed at 500 and 525 °C. In situ neutron diffraction experiments, as our studies on the SMARTS experiment despite the malfunctioning thermometry showed, are an ideal tool for this.

Finally, it is emphasized that critical consideration be made to experimental requirements and phase parameters for any future powder diffraction study on this system. In addition, the other parameters that can affect peak intensities (absorption, texture, thermal vibrations (Debye-Waller factors)) must be considered in order to properly extract quantitative phase information from collected diffraction data. It is to the authors knowledge that no direct measurement of the Debye-Waller factor for the γ′-U_2Mo phase has been made and in addition, only a few studies have published information on the Debye-Waller factor for the γ-phase in U–10Mo. It is suggested that the development of a theoretical prediction would be very useful for situations such as the one presented in this study, in addition to empirical determination.

CRediT authorship contribution statement

N.E. Peterson: Methodology, Formal analysis, Visualization, Writing - review & editing, Writing - original draft. **D. Malta:** Investigation, Formal analysis. **S.C. Vogel:** Investigation, Methodology, Formal analysis, Writing - review & editing. **B. Clausen:** Investigation, Methodology, Formal analysis, Writing - review & editing. **S. Jana:** Conceptualization, Project administration, Methodology, Investigation, Resources, Writing - review & editing. **V.V.**

Joshi: Conceptualization, Project administration, Resources, Writing - review & editing. **S.R. Agnew:** Funding acquisition, Conceptualization, Methodology, Supervision, Writing - review & editing.

Declaration of competing interest

The authors declare that they have no known competing financial interests or personal relationships that could have appeared to influence the work reported in this paper.

Acknowledgements

This work was funded by the U.S. Department of Energy National Nuclear Security Administration's Office of Material Management and Minimization and performed at Pacific Northwest National Laboratory under contract DE-AC05-76RL01830. The work has benefitted from the use of the Los Alamos Neutron Science Center (LANSCE) at Los Alamos National Laboratory. Los Alamos National Laboratory is operated by Triad National Security, LLC, for the National Nuclear Security Administration of the U.S. Department of Energy under contract number 89233218NCA000001.

Appendix A. Supplementary data

Supplementary data to this article can be found online at https://doi.org/10.1016/j.jnucmat.2020.152383.

References

[1] M.K. Meyer, J. Gan, J.F. Jue, D.D. Keiser, E. Perez, A. Robinson, D.M. Wachs, N. Woolstenhulme, G.L. Hofman, Y.S. Kim, Irradiation performance of U-Mo monolithic fuel, Nucl. Eng. Technol. 46 (2014) 169–182, https://doi.org/10.5516/NET.07.2014.706.
[2] G.L. Hofman, M.K. Meyer, S.C. Avenue, A.E. Ray, W. Lafayette, S. Paulo, Design of High Density Gamma-phase Uranium Alloys for LEU Dispersion Fuel Applications, 1998.
[3] J.H. Kittel, S.H. Paine, Effects of high burnup on natural uranium, Nucl. Sci. Eng. 3 (1958) 250–268.
[4] W.S. Blackburn, The effect of internal stresses due to irradiation growth and thermal cycling on the creep of uranium, in the cases of both elastic and plastic behaviour, J. Nucl. Energy - Parts A/B React. Sci. Technol. 14 (1961) 107–116, https://doi.org/10.1016/0368-3230(61)90099-4.
[5] B.R.T. Frost, R.W. Cahn, P. Haasen, E.J. Kramer, Materials Science and Technology: A Comprehensive Treatment, Nuclear Materials, VCH, 1994.
[6] K.H. Kim, D.B. Lee, C.K. Kim, G.E. Hofman, K.W. Paik, Characterization of U-2 wt % Mo and U-10 wt% Mo alloy powders prepared by centrifugal atomization, J. Nucl. Mater. 245 (1997) 179–184.
[7] A.A. Shoudy, W.E. McHugh, M.A. Silliman, The effect of irradiation temperature and fission rate on the radiation stability of the uranium-10 Wt.% molybdenum alloy, in: Radiat. Damage React. Mater. Part Proc. Symp. Radiat. Damage Solids React. Materz, 1963.
[8] R.M. Willard, A.R. Schmitt, Irradiation Swelling, Phase Reversion, and Intergranular Cracking of U-10 wt.% Mo Fuel Alloy (NAA-SR-8956), 1965.
[9] A. Devaraj, E. Kautz, L. Kovarik, S. Jana, N. Overman, C. Lavender, V.V. Joshi, Phase transformation of metastable discontinuous precipitation products to equilibrium phases in U10Mo alloys, Scripta Mater. 156 (2018) 70–74, https://doi.org/10.1016/j.scriptamat.2018.07.010.
[10] Y. Goldstein, A. Bar-Or, Decomposition OF gamma phase IN uranium alloys containing 8, 10.8, and 14.3 WT percent molybdenum, J. Inst. Met. 95 (1967) 17–21.
[11] C.A.W. Peterson, W.J. Steele, S.L. DiGiallonardo, Isothermal Transformation Study of Some Uranium-Base Alloys, Lawrence Radiation Lab., California. Univ., Livermore, 1964.
[12] P. Repas, R. Goodenow, R. Hehemann, Transformation characteristics of U-Mo and U-Mo-Ti alloys, Trans. Am. Soc. Met. 57 (1964) 150–163.
[13] D.B. Williams, E.P. Butler, Grain boundary discontinuous precipitation reactions, Int. Met. Rev. 26 (1981) 153–183.
[14] I. Manna, S.K. Pabi, W. Gust, Discontinuous reactions in solids, Int. Mater. Rev. 46 (2001) 53–91.
[15] A. Devaraj, L. Kovarik, E. Kautz, B. Arey, S. Jana, C. Lavender, V. Joshi, Grain boundary engineering to control the discontinuous precipitation in multicomponent U10Mo alloy, Acta Mater. 151 (2018) 181–190, https://doi.org/10.1016/j.actamat.2018.03.039.
[16] S. Jana, L. Sweet, D. Neal, A. Schemer-Kohrn, C. Lavender, V. Joshi, The role of ternary alloying elements in eutectoid transformation of U10Mo alloy part I. Microstructure evolution during arc melting and subsequent homogenization annealing in U9.8Mo0.2X alloy (X = Cr, Ni, Co), J. Nucl. Mater. 509 (2018) 318–329, https://doi.org/10.1016/j.jnucmat.2018.06.024.
[17] H.A. Saller, F.A. Rough, A.A. Bauer, Transformation Kinetics of Uranium-Molybdenum Alloys, Battelle Memorial Inst., Columbus, Ohio, 1954.
[18] W.A. Bostrom, M.W. Burkart, E.K. Halteman, R.D. Leggett, R.K. McGeary, T.R. Padden, Development and Properties of Uranium-Base Alloys Corrosion Resistant in High Temperature Water. Part I. Alloys without Protective Cladding, Westinghouse Electric Corp. Atomic Power Div., Pittsburgh, 1955.
[19] R.J. Van Thyne, D.J. McPherson, Transformation kinetics of uranium-molybdenum alloys, Trans. ASM 49 (1957) 598–621.
[20] S. Säubert, R. Jungwirth, T. Zweifel, M. Hofmann, M. Hoelzel, W. Petry, Neutron and hard X-ray diffraction studies of the isothermal transformation kinetics in the research reactor fuel candidate U-8 wt%Mo, J. Appl. Crystallogr. 49 (2016) 923–933, https://doi.org/10.1107/S1600576716005744.
[21] M.A. Steiner, C.A. Calhoun, R.W. Klein, K. An, E. Garlea, S.R. Agnew, α-Phase transformation kinetics of U - 8 wt% Mo established by in situ neutron diffraction, J. Nucl. Mater. (2016), https://doi.org/10.1016/j.jnucmat.2016.05.016.
[22] S. Jana, A. Devaraj, L. Kovarik, B. Arey, L. Sweet, T. Varga, C. Lavender, V. Joshi, Kinetics of cellular transformation and competing precipitation mechanisms during sub-eutectoid annealing of U10Mo alloys, J. Alloys Compd. (2017), https://doi.org/10.1016/j.jallcom.2017.06.292.
[23] H.-R. Wenk, L. Lutterotti, S.C. Vogel, Rietveld texture analysis from TOF neutron diffraction data, Powder Diffr. 25 (2010) 283–296, https://doi.org/10.1154/1.3479004.
[24] S. Takajo, S.C. Vogel, Determination of pole figure coverage for texture measurements with neutron time-of-flight diffractometers, J. Appl. Crystallogr. 51 (2018) 895–900.
[25] A.S. Losko, S.C. Vogel, H.M. Reiche, H. Nakotte, A six-axis robotic sample changer for high-throughput neutron powder diffraction and texture measurements, J. Appl. Crystallogr. 47 (2014) 2109–2112.
[26] M.A.M. Bourke, D.C. Dunand, E. Ustundag, SMARTS–a spectrometer for strain measurement in engineering materials, Appl. Phys. A 74 (2002) s1707–s1709.
[27] L. Lutterotti, S. Matthies, H.-R. Wenk, MAUD (material analysis using diffraction): a user friendly Java program for Rietveld texture analysis and more, in: Proceeding Twelfth Int. Conf. Textures Mater., NRC Research Press Ottowa, Canada, 1999, p. 1599.
[28] A.C. Larson, R.B. Von Dreele, GSAS: General Structure Analysis System, Los Alamos National Laboratory, Los Alamos, NM, 1986. Report LAUR 86-748.
[29] S.C. Vogel, gsaslanguage: a GSAS script language for automated Rietveld refinements of diffraction data, J. Appl. Crystallogr. 44 (2011) 873–877.
[30] F. Bachmann, R. Hielscher, H. Schaeben, Texture analysis with MTEX–free and open source software toolbox, in: Solid State Phenom., Trans Tech Publ, 2010, pp. 63–68.
[31] L.-M. Peng, G. Ren, S.L. Dudarev, M.J. Whelan, Debye–Waller factors and absorptive scattering factors of elemental crystals, Acta Crystallogr. A Found. Crystallogr. 52 (1996) 456–470.
[32] A.E. Austin, Carbon positions in uranium carbides, Acta Crystallogr. 12 (1959) 159–161.
[33] A.C. Lawson, J.A. Goldstone, B. Cort, R.I. Sheldon, E.M. Foltyn, Debye-Waller Factors of the Light Actinide Metals, Los Alamos National Lab., 1993.
[34] A. Perricone, H. Noël, Crystal structure refinements and magnetic behavior of U6Ni, UNi5, UNi2 and the substitution derivative UNi1. 7Si0. 3, Chem. Met. Alloy (2008) 54–57.
[35] B.H. Toby, R.B. Von Dreele, GSAS-II: the genesis of a modern open-source all purpose crystallography software package, J. Appl. Crystallogr. 46 (2013) 544–549.
[36] J. Rest, Y.S. Kim, G.L. Hofman, M.K. Meyer, S.L. Hayes, U-mo Fuels Handbook. Version 1.0, Argonne National Lab.(ANL), Argonne, IL (United States), 2006.
[37] S. Jana, N. Overman, T. Varga, C. Lavender, V. V Joshi, Phase transformation kinetics in rolled U-10 wt.% Mo foil: effect of post-rolling heat treatment and prior γ-UMo grain size, J. Nucl. Mater. 496 (2017) 215–226.
[38] B.T.M. Willis, A.W. Pryor, Thermal Vibrations in Crystallography, Cambridge University Press, Cambridge, 1975.
[39] M.S. Blanter, V.P. Glazkov, V.A. Somenkov, V.K. Orlov, A. V Laushkin, The effect of alloying on thermal displacements in uranium and plutonium alloys and the mechanism of stabilization of high-temperature phases by alloying, Phys. Met. Metallogr. 101 (2006) 153–158.
[40] N.J. Lane, S.C. Vogel, G. Hug, A. Togo, L. Chaput, L. Hultman, M.W. Barsoum, Neutron diffraction measurements and first-principles study of thermal motion of atoms in select M n+ 1 A X n and binary M X transition-metal carbide phases, Phys. Rev. B 86 (2012) 214301.
[41] S. Neogy, M.T. Saify, S.K. Jha, D. Srivastava, M.M. Hussain, G.K. Dey, R.P. Singh, Microstructural study of gamma phase stability in U–9 wt.% Mo alloy, J. Nucl. Mater. 422 (2012) 77–85.
[42] J.-S. Lee, C.-H. Lee, K.H. Kim, V. Em, Study of decomposition and reactions with aluminum matrix of dispersed atomized U-10 wt% Mo alloy, J. Nucl. Mater. 306 (2002) 147–152.